Supplementary Information

In Situ 2D MoS_2 Field Effect Transistors with an Electron Beam Gate

Paul Masih Das[1], Marija Drndic[1]*

[1]Department of Physics and Astronomy, University of Pennsylvania, Philadelphia, Pennsylvania 19104, USA.

*Correspondence to: drndic@physics.upenn.edu.

Section S1. Full discussion of electron-induced radiolysis, knock-on, and thermal excitations in SiN_x membranes.

Electron irradiation of insulating TEM specimens has been studied previously and results in radiation damage through primarily three modes: knock-on collisions, radiolysis, and electrostatic charging.[1–3] In the former, atoms in the specimen get displaced *via* momentum transfer with energetic 200 keV electrons, resulting in defects and vacancies.[4] It is well-known that ejecting N atoms from SiN_x results in the formation of positively-charged K^+ centers, which give rise to a multitude of charge trap states.[5,6] While a population of charge traps in the window region could potentially lead to I_{ds} modulation, the spatial positions of K^+ centers are fixed[5,6] and therefore unlikely to cause the gating effect that is observed to be independent of the TEM beam location (see **Figure 3**). In the case of radiolysis, incident electrons cause in-plane vibrational excitations within the specimen, which lead to a localized temperature increase. While a thermoelectric effect has been previously demonstrated in MoS_2 and would explain the correlation here between I_{ds} and I_{beam}, we calculate an estimated heat dissipation time of ~ 400 ms, which is inconsistent by over three orders of magnitude with the observed decay in I_{ds} shown in **Figure 2b**. Both knock-on collisions and radiolysis are hence not likely causes of the observed gating effect.

In the case of electrostatic charging, the ejection of secondary and Auger electrons from the insulating specimen due to TEM beam irradiation leads to a charge imbalance. In particular, the time-dependent charge diffusion in amorphous SiN_x membranes has been studied using *In Situ* X-ray diffraction.[7] Assuming constant temperature, the relationship between charge population (I) and time (t) is given by:

$$I(t) \propto exp(-Ct)$$

Where C is a constant given by $1/\tau$ (τ = characteristic time constant). Charge in the SiN_x window therefore decays exponentially with time. This is in excellent agreement with the time-dependent DC measurement in **Figure 2b** (orange curve) where the exponential curve shown in black fits well to the I_{ds} curve after the electron beam is turned off (*i.e.,* discharging). The converse (*i.e.,* charging) is observed when the electron beam is turned on (**Supplementary Figure S3**).

This suggests that the suppression of I_{ds} in a TEM-FET's MoS_2 channel when the electron beam is turned on is due to the presence of a positive surface potential on the SiN_x window caused

by electrostatic charging. The strength of this potential is directly proportional to the flux of incident electrons, which explains why stronger current suppression is observed at higher I_{beam} values (**Figures 3-5**). Unlike K^+ centers caused by N vacancies, the delocalized nature of these charges leads to a uniform gating effect that is independent of electron beam location on the window (**Figure 3**). Furthermore, placing the TEM beam *off* the SiN_x window prevents secondary and Auger electron ejection due to the underlying Si substrate, which eliminates charging and any subsequent gating effect (**Figure 4**). Although further studies are needed, it is probable that larger $\Delta G/G$ values are observed when exposing MoS_2-covered SiN_x (see **Figure 3**) due to the existence of charge trap states at the MoS_2-SiN_x interface.

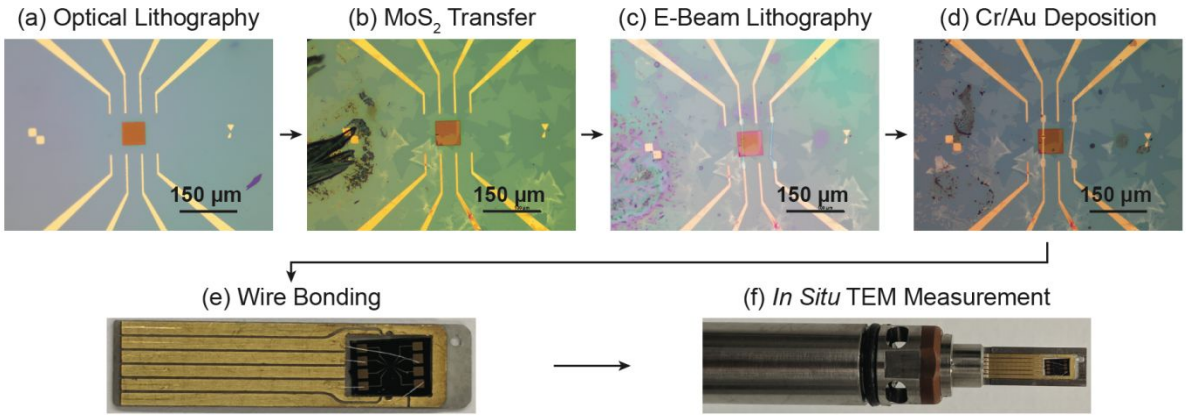

Figure S2. TEM-FET fabrication process. (a) Using optical lithography and microfabrication, 60 µm wide TEM windows are first produced in the center of 3 mm × 5 mm Si/SiN_x substrates. Electrical leads and contact pads are then aligned and deposited adjacent to the window. (b) PMMA-covered MoS_2 flakes grown *via* chemical vapor deposition are positioned using an optical microscope and transferred on top of the window. After PMMA removal in hot (90°C) acetone, (c) samples get coated with fresh PMMA and patterned with electron beam lithography. (d) 5 nm/40 nm of Cr/Au are then put down using physical vapor deposition. (e) The Si/SiN_x chip then undergoes mounting (Ag paint) and wire bonding (Al wire) to a ceramic chip carrier, which is (f) placed in a 6-lead electrical biasing holder (Hummingbird Scientific) for *In Situ* measurements.

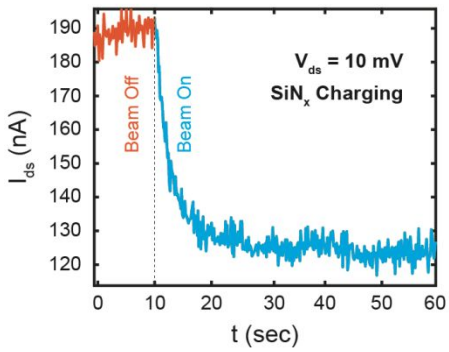

Figure S3. Continuous two-terminal DC measurement of a 2D channel, reflecting SiN_x membrane charging. Time-dependent I_{ds} measurement of an TEM-FET with L_{ch} = 2.2 μm under a fixed bias voltage (V_{ds} = 10 mV). After 10 seconds (orange curve), the electron beam was turned on (blue curve). As discussed in the main text, the resulting drop in I_{ds} is indicative of a reduction in current across the MoS_2 channel due to charging (positive surface potential) of the SiN_x membrane.

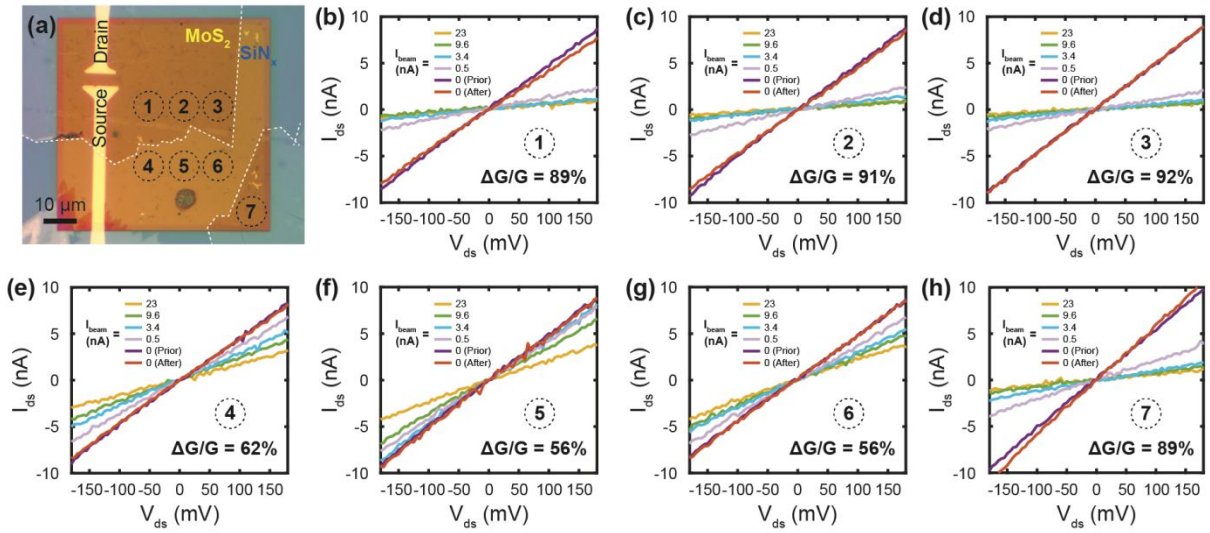

Figure S4. Full two-terminal data corresponding to exposed locations in Figure 3. (a) Optical image of the TEM-FET shown in **Figure 3** of the main text with 7 circles indicating the different positions of the electron beam (d_{beam} = 8.7 μm) on the SiN_x window. The edges of two different MoS_2 flakes in the top left and bottom right regions (darker color on the substrate) are outlined in white. I_{ds}-V_{ds} curves for different I_{beam} values at positions (b) 1, (c) 2, (d) 3, (e) 4, (f) 5, (g) 6, and (h) 7. The distance of the electron beam from the transistor channel does not influence device conductance during the timescales of our measurements. However, whether the beam hits SiN_x-supported MoS_2 or just the bare SiN_x window (lighter color in (a)) is strongly correlated to ΔG/G. As shown at positions 1, 2, 3, and 7, larger ΔG/G values (90 ± 1.3 %) are obtained for electron beam exposure to MoS_2/SiN_x compared to the bare SiN_x window (58 ± 2.8 %) at positions 4, 5, and 6.

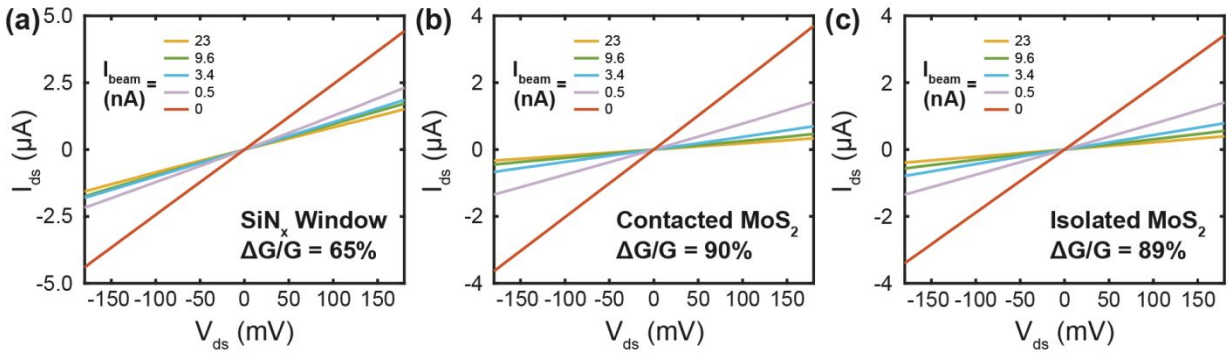

Figure S5. Transport properties during electron-beam irradiation of electrically-isolated MoS_2 flakes. (a) I_{ds}-V_{ds} curves for an TEM-FET with L_{ch} = 2.2 μm under electron beam exposure of the bare SiN_x window. (b) Transport characteristics of a device where the electron beam is exposing MoS_2 that is in contact with Cr/Au leads. (c) Data for a sample under exposure of electrically-isolated MoS_2 flakes (*i.e.,* flakes that are not in contact with the electrodes). The configuration of the exposed MoS_2 (*i.e.,* contacted or isolated MoS_2) produces a negligible difference in ΔG/G. In (b) and (c), the electron beam is hitting the substrate surface adjacent to, but not directly on the MoS_2 channel as shown in **Figure 4** of the main text.

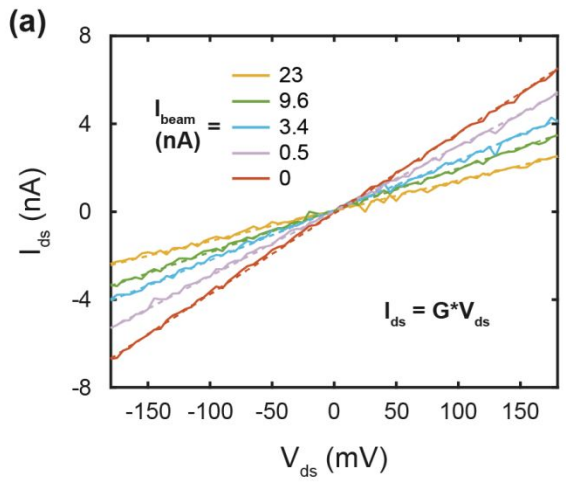

(b)

I_{beam} (nA)	G (nS)	σ (nS)	2σ (nS)
0	45.8	0.15	0.30
0.5	36.9	0.16	0.33
3.4	28.5	0.17	0.35
9.6	23.8	0.16	0.32
23	17.1	0.18	0.36

Figure S6. Standard error intervals for conductance quantification. (a) I_{ds}-V_{ds} curves for an example TEM-FET at different I_{beam} values. Raw data are the solid lines while linear fits for device conductance are shown graphically as dashed lines. (b) Table showing acquired values for G (second column) at each I_{beam} current (first column) using a linear regression. Across different curves, we observe a standard error (σ) of 0.16 ± 0.01 nS (third column), which corresponds to a prediction interval of approximately 68%. 2σ values (fourth column) for a prediction interval of 95% are also given. Other TEM-FET devices display comparable or lower values of 2σ. This error most likely arises from electromagnetic variations inside the objective lens of the TEM or from electronic noise in the transport measurement setup. Additional information on data acquisition and analysis can be found in the Methods section.

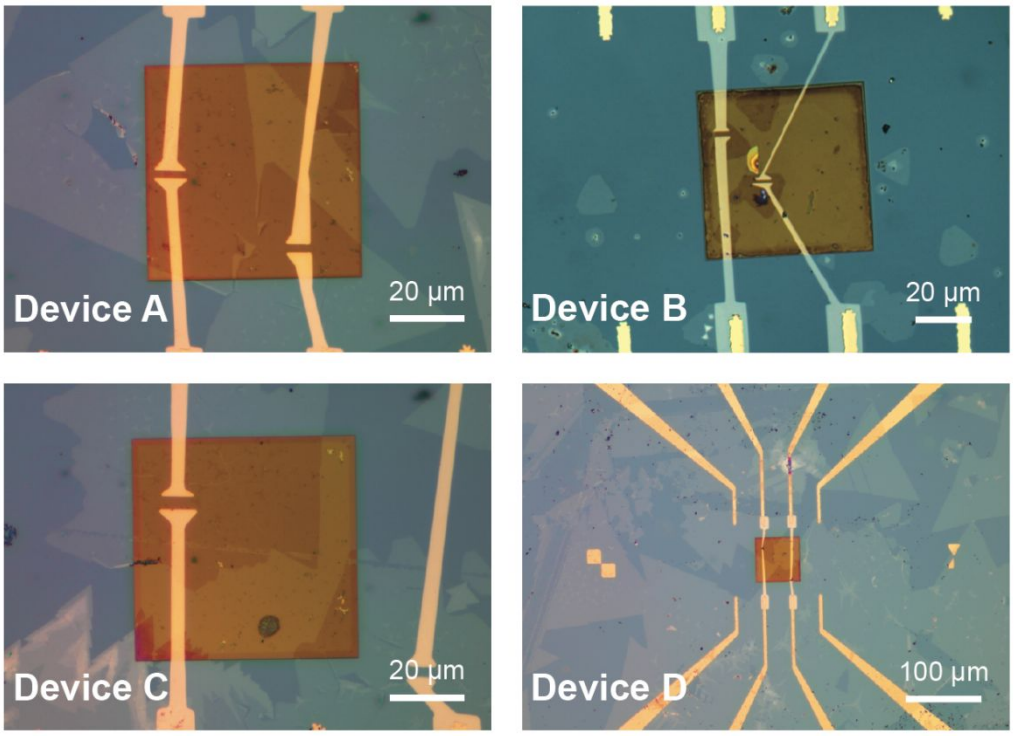

Figure S7. Optical images of various TEM-FET devices. (a-d) Optical images of four separate TEM-FET devices comprised of two-terminal contacted monolayer MoS_2 flakes on a 100 nm thick low-stress SiN_x window. Electrical contacts were patterned with electron beam lithography after 2D flake transfer and composed of 40 nm Au on top of a 5 nm Cr adhesion layer. Full details of the fabrication process can be found in the Methods and **Supplementary Figure S2**.

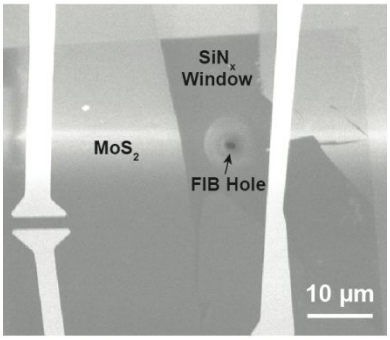

Figure S8. SEM characterization of TEM-FET containing a single FIB hole through the SiN_x window. SEM image of the device shown in **Figure 5b-d** consisting of a two-terminal contacted MoS_2 flake (light gray) on a SiN_x window (dark gray) containing a 1.2 µm diameter hole. The hole was fabricated using a Ga^+ focused ion beam operating at 30 keV with a 10 pA current. During the set of I_{ds}-V_{ds} measurements shown in **Figure 2c**, the electron beam was incident entirely through the FIB hole (*i.e.,* no interaction with the SiN_x membrane).

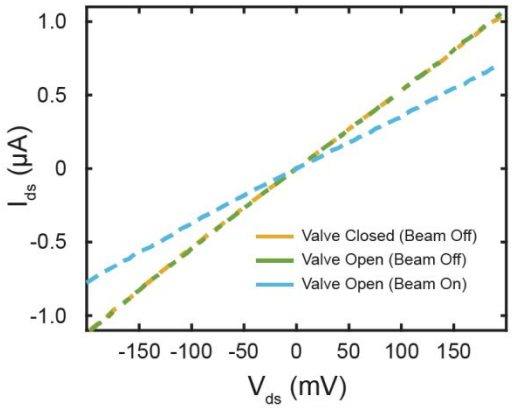

Figure S9. Dependence of I_{ds}-V_{ds} on beam valve state. I_{ds}-V_{ds} curves for a TEM-FET device with the beam valve closed (orange) and open (green, blue). The state of the beam valve has a negligible effect (*i.e.,* below the noise limit) on G. A TEM beam valve is a physical isolation valve separating the electron gun chamber ($p \sim 10^{-8}$ Pa) from the main specimen chamber ($p \sim 10^{-6}$ Pa).

References

(1) Algara-Siller, G.; Kurasch, S.; Sedighi, M.; Lehtinen, O.; Kaiser, U. The Pristine Atomic Structure of MoS_2 Monolayer Protected from Electron Radiation Damage by Graphene. *Appl. Phys. Lett.* **2013**, *103*, 203107.

(2) Egerton, R. F.; Li, P.; Malac, M. Radiation Damage in the TEM and SEM. *Micron* **2004**, *35*, 399–409.

(3) Jiang, N.; Spence, J. C. H. On the Dose-Rate Threshold of Beam Damage in TEM. *Ultramicroscopy* **2012**, *113*, 77–82.

(4) Masih Das, P.; Thiruraman, J. P.; Zhao, M.-Q.; Mandyam, S.; Johnson, A. T. C.; Drndić, M. Atomic-Scale Patterning in Two-Dimensional Van der Waals Superlattices. *Nanotechnology* **2019**, *31*, 105302.

(5) Sharma, V.; Tracy, C.; Schroder, D.; Flores, M.; Dauksher, B.; Bowden, S. Study and Manipulation of Charges Present in Silicon Nitride Films. *IEEE PVSC* **2013**, *39,* 1288–1293.

(6) Chen, K.; Kiriya, D.; Hettick, M.; Tosun, M.; Ha, T.; Madhvapathy, S. R.; Desai, S.; Sachid, A.; Javey, A. Air Stable N-Doping of WSe_2 by Silicon Nitride Thin Films with Tunable Fixed Charge Density. *APL Mater.* **2014**, *2*, 092504.

(7) Pelleg, J. *Solid Mechanics and Its Applications*; Barber, J., Klarbring, A., Eds.; Springer: New York, **2016**; pp 413–444.